Offline Identification of Differential Inductances in PMSMs: Experimental and Simulation-Based Comparison

1st Timo Hörmann
Institute Electrical Machines (IEM)
RWTH Aachen University
Aachen, Germany
timo.hoermann@iem.rwth-aachen.de

2nd Sebastian Mönninghoff
Institute Electrical Machines (IEM)
RWTH Aachen University
Aachen, Germany
sebastian.moenninghoff@iem.rwth-aachen.de

3rd Simon Steentjes
Institute Electrical Machines (IEM)
RWTH Aachen University
Aachen, Germany
simon.steentjes@iem.rwth-aachen.de

***Abstract*—When permanent magnet synchronous machines (PMSMs) operate under high utilization, magnetic saturation introduces pronounced nonlinearities – especially during transients. While absolute inductances adequately describe steady-state behavior, they fall short in capturing the machine's dynamics during rapid current changes. This shortcoming is critical in sensorless control strategies that rely on high-frequency current injection for rotor position estimation. To accurately model transient behavior under these conditions, differential inductances are essential, as they account for the dynamic effects that absolute inductances cannot.**

Differential inductances can be determined either through finite element (FE) simulations or via experimental identification, as demonstrated in this work. Two identification methods are implemented and validated on a dedicated test bench. The experimentally obtained values are then compared with results from the institute's in-house FE simulation tool *pyMOOSE*. Notably, the derivative based identification shows the best overall performance, offering a superior accuracy and robustness across the full operating range when benchmarked against the FE results.

***Index Terms*—identification, parameters, differential inductances, permanentmagnet synchronous machines, sensorless, modeling**

I. Introduction

Permanent magnet synchronous machines (PMSMs) are widely used today. While current-dependent fundamental-wave models account for magnetic saturation and nonlinearities, they fall short for accurately modeling transient behavior [1], [2], [3]. Such transients arise, for example, from high-frequency current injection in sensorless control schemes or as a result of the pulsed voltage waveforms produced by voltage source inverters. To effectively model these effects, a representation based on differential inductances is essential [4].

Fig. 1 illustrates the difference between absolute and differential inductances. The discrepancy becomes particularly pronounced under magnetic saturation. While the absolute inductance L is defined as the ratio of flux linkage Ψ to current i, $\frac{\Psi}{i}$, the differential inductance L_{diff} is given by the derivative of the flux linkage with respect to current i, $\frac{\mathrm{d}\Psi}{\mathrm{d}i}$, providing a more accurate representation of the machine behavior under transient conditions [1] and [5]. This representation also enables to analyze of effects such as optimizing the switching angles to improve the overall efficiency as shown in [3]. Moreover, differential inductances are a key requirement for rotor position estimation using high-frequency injection methods in sensorless control schemes [4], [6]. The position is obtained in the $\alpha\beta$-system via

$$\mathbf{L} = \mathbf{L}_{\mathrm{c}} + \mathbf{L}_{\mathrm{a}}(\varphi) = \begin{bmatrix} \frac{L_{\mathrm{dd}}+L_{\mathrm{qq}}}{2} & \frac{L_{\mathrm{dq}}-L_{\mathrm{qd}}}{2} \\ \frac{L_{\mathrm{qd}}-L_{\mathrm{dq}}}{2} & \frac{L_{\mathrm{dd}}+L_{\mathrm{qq}}}{2} \end{bmatrix} + \begin{bmatrix} -\frac{L_{\mathrm{qq}}-L_{\mathrm{dd}}}{2} & -\frac{L_{\mathrm{qd}}+L_{\mathrm{dq}}}{2} \\ \frac{L_{\mathrm{dq}}+L_{\mathrm{qd}}}{2} & \frac{L_{\mathrm{dd}}-L_{\mathrm{qq}}}{2} \end{bmatrix} \begin{bmatrix} \cos(2\varphi) & \sin(2\varphi) \\ \sin(2\varphi) & -\cos(2\varphi) \end{bmatrix}, \tag{1}$$

as outlined in [6] and [4]. The inductance matrix $\mathbf{L}$ comprises a constant part $\mathbf{L}_{\mathrm{c}}$ and a component $\mathbf{L}_{\mathrm{a}}$ that varies in the $\alpha\beta$-system with the rotor angle φ. Whereas L_{dd} and L_{qq} are the so-called self-inductances and L_{dq} and L_{qd} the coupling inductances of the PMSM.

The differential inductances can be obtained either *online*, during normal operation, or *offline*, during a dedicated measurement. An online identification method, proposed in [7], is based on a long-term memory recursive least squares (RLS) algorithm to estimate the flux linkages and differential inductances. However, this approach requires several seconds to converge and depends on a few initialization parameters. Another online identification method is presented in [8], which estimates the differential inductances L_{dd} and L_{qq} at standstill or low speeds during current transients. In addition, data-driven approaches have also been proposed, such as in [9], although their applicability can be limited due to the need for large and representative training datasets.

Despite the capabilities of online parameter estimation, offline methods are still required, for instance, to verify the FE simulation or to establish a basic parameterization of the control structure. This paper aims to provide a comprehensive overview of two offline identification methods [10], [11] and [12], encompassing both measurement-based approaches

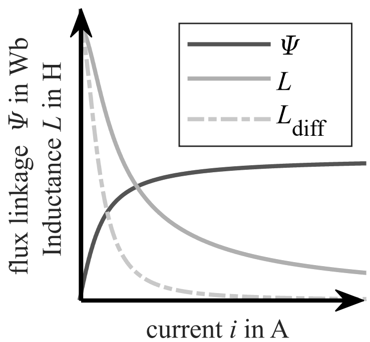

Fig. 1: A schematic illustration of the flux saturation behavior caused by high currents is presented, together with the corresponding absolute inductance L and differential inductance L_{diff}.

and finite element (FE) simulation techniques. These two measurement-based identification methods are implemented and compared on a rapid control prototyping system using two different electrical machines to demonstrate the general applicability of the methods. Furthermore, the experimentally determined inductances are compared with those obtained from FE simulations. The FE simulations are performed using the institute's in-house solver *pyMOOSE*.

II. Current- and Angle-Dependent dq-Model

The general representation of permanent magnet synchronous machines (PMSMs) in the common rotating dq-system is given by

$$u_{\mathrm{d}} = Ri_{\mathrm{d}} + \frac{\mathrm{d}}{\mathrm{dt}}\Psi_{\mathrm{d}} - \omega\Psi_{\mathrm{q}} \tag{2}$$

$$u_{\mathrm{q}} = Ri_{\mathrm{q}} + \frac{\mathrm{d}}{\mathrm{dt}}\Psi_{\mathrm{q}} + \omega\Psi_{\mathrm{d}} \tag{3}$$

where $u_{\mathrm{d,q}}$ and $i_{\mathrm{d,q}}$ denote the stator voltages and currents in the dq-system, respectively, $\Psi_{\mathrm{d,q}}$ represent the corresponding flux linkages, and R is the stator phase resistance assuming that all three phases are symmetrical. The electrical angular velocity ω is related to the rotor electrical angle φ by $\omega = \frac{\mathrm{d}\varphi}{\mathrm{dt}}$. For the sake of completeness, it should be noted that voltage and current are time-dependent quantities. However, to maintain clarity and readability, explicit time notation is omitted throughout this work.

In practice, the flux linkages $\Psi_{\mathrm{d,q}}$ are not constant but are dependent on various operating conditions, including the stator currents, rotor position φ, temperature ϑ, aging effects, and time t. This leads to the generalized dependency $\Psi_{\mathrm{d,q}} = \Psi_{\mathrm{d,q}}(i_{\mathrm{d}}, i_{\mathrm{q}}, \vartheta, \varphi, t, \dots)$. In this work, the analysis is restricted to the current and angular dependency of the flux linkages. Temperature effects are considered neglible due to the controlled and stable thermal conditions maintained during all identification procedures. Since these methods focus on the short-term behavior, long-term effects suchs time- and aging-related changes are also disregarded. Consequently, the flux linkages being expressed as $\Psi_{\mathrm{d,q}} = \Psi_{\mathrm{d,q}}(i_{\mathrm{d}}, i_{\mathrm{q}}, \varphi)$.

For many applications, it is sufficient to employ the simplified linear fundamental-wave dq-model

$$u_{\mathrm{d}} = Ri_{\mathrm{d}} + L_{\mathrm{d}}\frac{\mathrm{d}}{\mathrm{dt}}i_{\mathrm{d}} - \omega L_{\mathrm{q}} i_{\mathrm{q}} \tag{4}$$

$$u_{\mathrm{q}} = Ri_{\mathrm{q}} + L_{\mathrm{q}}\frac{\mathrm{d}}{\mathrm{dt}}i_{\mathrm{q}} + \omega(L_{\mathrm{d}} i_{\mathrm{d}} + \Psi_{\mathrm{PM}}). \tag{5}$$

However, to accurately capture transient events - particularly in saliency-based sensorless control techniques [6] - the fundamental-wave model must be extended to include differential inductances. These inductances

$$\begin{aligned} L_{\mathrm{dd}} &= \frac{\partial\Psi_{\mathrm{d}}}{\partial i_{\mathrm{d}}} \quad L_{\mathrm{dq}} = \frac{\partial\Psi_{\mathrm{d}}}{\partial i_{\mathrm{q}}} \quad \Lambda_{\mathrm{d}} = \frac{\partial\Psi_{\mathrm{d}}}{\partial\varphi} \\ L_{\mathrm{qd}} &= \frac{\partial\Psi_{\mathrm{q}}}{\partial i_{\mathrm{d}}} \quad L_{\mathrm{qq}} = \frac{\partial\Psi_{\mathrm{q}}}{\partial i_{\mathrm{q}}} \quad \Lambda_{\mathrm{q}} = \frac{\partial\Psi_{\mathrm{q}}}{\partial\varphi} \end{aligned} \tag{6}$$

represent the partial derivatives of the flux linkages with respect to the d- and q-axis currents, as well as the rotor position φ.

Substituting the expressions from (6) into the general model (2) and (3) yields the extended dq-model [2]:

$$u_{\mathrm{d}} = Ri_{\mathrm{d}} + L_{\mathrm{dd}}\frac{\mathrm{d}}{\mathrm{dt}}i_{\mathrm{d}} + L_{\mathrm{dq}}\frac{\mathrm{d}}{\mathrm{dt}}i_{\mathrm{q}} - \omega(\Lambda_{\mathrm{d}} - \Psi_{\mathrm{q}}) \tag{7}$$

$$u_{\mathrm{q}} = Ri_{\mathrm{q}} + L_{\mathrm{qd}}\frac{\mathrm{d}}{\mathrm{dt}}i_{\mathrm{d}} + L_{\mathrm{qq}}\frac{\mathrm{d}}{\mathrm{dt}}i_{\mathrm{q}} + \omega(\Lambda_{\mathrm{q}} + \Psi_{\mathrm{d}}). \tag{8}$$

This approach not only captures the current-dependent flux linkages under steady-state conditions, but also transient events caused by current variations and changes in rotor position.

III. Offline-Identification Methods

A. Derivative Method

The derivative method utilizes the relationship shown in (6) to determine the differential inductances. These inductances can also be obtained from FE simulations or from data collected on the test bench. The identification process on the test bench is described as follows. The machine-under-test is kept at a constant speed by means of a speed-controlled load machine. It is also assumed that the current control loop is capable of imposing constant dq-currents to the machine-under-test. In this case, the flux derivatives in (2) and (3) disappear, and by rearranging, it is possible to express the flux linkages as

$$\Psi_{\mathrm{d}} = \frac{u_{\mathrm{q}} - Ri_{\mathrm{q}}}{\omega} \tag{9}$$

$$\Psi_{\mathrm{q}} = -\frac{u_{\mathrm{d}} - Ri_{\mathrm{q}}}{\omega}, \tag{10}$$

where only the voltages $u_{\mathrm{d,q}}$ and the phase resistance R are required, since the currents $i_{\mathrm{d,q}}$ are already required for the current control loop and are therefore always available. Due to its strong temperature dependence, the phase resistance must be appropriately accounted for. This is achieved by maintaining a constant temperature during the measurement process. As previously mentioned, the differential inductances $L_{\mathrm{dd}}, L_{\mathrm{dq}}, L_{\mathrm{qd}}, L_{\mathrm{qq}}, \Lambda_{\mathrm{d}}$, and Λ_{q} are determined by means of partial differentiation.

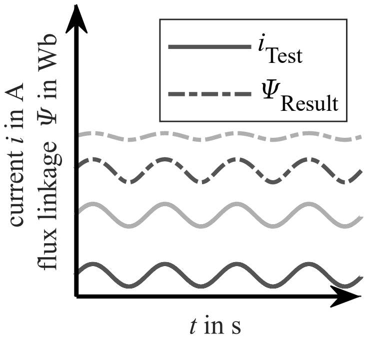

Fig. 2: A schematic current profile is shown: the dark grey region corresponds to a test current with a low steady-state value, while the light grey region represents a higher steady-state current. The dashed lines indicate the resulting flux responses.

B. High Frequency Current Method

Another method, proposed in [12], is applicable to real machines but only at standstill. For high-torque PMSMs, this requires significant effort to block the rotor - either by mechanical blocking or using a suitable load machine. The method involves applying various current combinations, supplemented by a high-frequency component. By exploiting the saturation behavior of the machine, the differential inductances can be identified. Fig. 2 shows two schematics of injected currents along their corresponding flux responses. Both have identical amplitude and frequency and differ by their steady-state current levels. This shift results in operation in higher or lower positions on the saturation curve, leading to distinct flux results. Consequently, the inductances can be calculated.

The differential inductances are determined by superimposing a high-frequency current $i_{\mathrm{x,HF}}$, where $x \in \{d, q\}$, onto constant baseline currents that define the operating point. Since the rotor is blocked, the condition $\omega \stackrel{!}{=} 0$ is satisfied, (7) and (8) simplify to

$$u_{\mathrm{d}} = Ri_{\mathrm{d}} + L_{\mathrm{dd}}\frac{\mathrm{d}}{\mathrm{dt}}i_{\mathrm{d}} + L_{\mathrm{dq}}\frac{\mathrm{d}}{\mathrm{dt}}i_{\mathrm{q}} \tag{11}$$

$$u_{\mathrm{q}} = Ri_{\mathrm{q}} + L_{\mathrm{qd}}\frac{\mathrm{d}}{\mathrm{dt}}i_{\mathrm{d}} + L_{\mathrm{qq}}\frac{\mathrm{d}}{\mathrm{dt}}i_{\mathrm{q}} \tag{12}$$

The derivation procedure is illustrated hereafter using the d-axis as a representative example. Adding $i_{\mathrm{d,HF}}$ to (12) and taking into account that $\frac{\mathrm{d}}{\mathrm{dt}}i_{\mathrm{q}} = 0$, leads to

$$u_{\mathrm{d,0}} + u_{\mathrm{d,HF}} = R(i_{\mathrm{d,0}} + i_{\mathrm{d,HF}}) + L_{\mathrm{dd}}\frac{\mathrm{d}}{\mathrm{dt}}i_{\mathrm{d,HF}}. \tag{13}$$

The bias

$$u_{\mathrm{d,0}} = Ri_{\mathrm{d}} \tag{14}$$

resulting from the constant voltage $u_{\mathrm{d,0}}$ and constant current $i_{\mathrm{d,0}}$ must be separated from the high-frequency component $i_{\mathrm{d,HF}}$ using appropriate filtering methods, as detailed in section IV-B.

At high frequencies, the machine behaves as a complex impedance, allowing analysis using standard AC circuit theory. After removing the DC component, (13) can be rewritten as follows:

$$\underline{U}_{\mathrm{d,HF}} = R\underline{I}_{\mathrm{d,HF}} + j\omega_{\mathrm{HF}}L_{\mathrm{dd}}\underline{I}_{\mathrm{d,HF}}. \tag{15}$$

Here, ω_{HF} represents the angular frequency of the injected test signal instead of the angular velocity of the permanent magnet synchronous machine. By rearranging (15), the differential inductances can be obtained:

$$L_{\mathrm{dd}} = \frac{1}{\omega_{\mathrm{HF}}}\sqrt{\frac{U_{\mathrm{d,HF}}^2}{I_{\mathrm{d,HF}}^2} - R^2} \tag{16}$$

$$L_{\mathrm{qd}} = \frac{U_{\mathrm{d,HF}}}{\omega_{\mathrm{HF}}I_{\mathrm{q,HF}}}. \tag{17}$$

These can be calculated using the amplitudes of the injected voltage and resulting current. By injecting a high-frequency current into the q-axis $i_{\mathrm{q,HF}}$ instead of the d-axis, the remaining differential inductances can be determined

$$L_{\mathrm{qq}} = \frac{1}{\omega_{\mathrm{HF}}}\sqrt{\frac{U_{\mathrm{q,HF}}^2}{I_{\mathrm{q,HF}}^2} - R^2} \tag{18}$$

$$L_{\mathrm{dq}} = \frac{U_{\mathrm{q,HF}}}{\omega_{\mathrm{HF}}I_{\mathrm{d,HF}}}. \tag{19}$$

It can be observed that the self-inductances L_{dd} and L_{qq} depend solely on their respective voltages and currents, while the cross-coupling inductances, also often referred to as mutual inductances, are influenced by the cross-axis components. This method originates from [1], [12], and [13]. It is important to note that in order to capture the angular dependencies, the entire identification process must be performed at each rotor angle position. Since this method is applied at stillstand, it cannot account for the rotor angle dependend differential inductances Λ_{d} and Λ_{q}.

IV. Implementation and Execution

A. Current Control Structure and Testbench Setup

A current control loop is necessary for determining the differential inductances using both methods. The setpoint for the current control loop is superimposed with a high-frequency component. The current control loop is implemented on a dSPACE Scalexio hardware, which serves as a rapid control prototyping platform.

The tests are performed on a test bench consisting of a load machine and the machine-under-test. The machines are mechanically coupled, with the load machine being speed-controlled to ensure a constant speed, which is required for the derivative method, described in section III-A. For the method described in section III-B, the speed setpoint is set to zero, meaning the machine operates at standstill. The machine-under-test is supplied via a voltage source inverter. A power analyzer records the phase voltages and currents, as well as the rotor position provided by an encoder. The hardware used is listed in Table I. The control signals are often used for parameter identification, however; this can lead to errors, as the voltage output by the control loop does not necessarily match the actual voltage applied to the machine. This discrepancy arises from inverter dead time - implemented to prevent short circuits in the half-bridge - as well as voltage drops caused by free-wheeling diodes, switching losses and resistance of supply cables, as discussed in [14].

B. Analysis and Filtering

As noted in section IV-A, the machine-under-test is powered by a voltage inverter, which introduces harmonic components into the measured signals. To extract only the fundamental wave, theses signals must be filtered and only complete electrical periods should be considered. In the dq-reference frame, simple averaging is sufficient for fundamental wave extraction. However, this approach is not suitable when identifying angle-dependent differential inductances.

Angular dependencies, such as those caused by slotting effects [5], introduce addtional harmonics in the dq-system. To eliminate current harmonics caused by switching events, the current signal is smoothed using a moving average filter with a window size of $n = 1/(f_{\mathrm{switching}} t_{\mathrm{sample}})$, where $f_{\mathrm{switching}}$ is the switching frequency of the inverter and t_{sample} is the sampling period of the power analyzer. Fig. 3 shows current measurements at an examplary operating point, recorded by the power analyzer, along with the subsequently filtered currents. This filtering method ensures that all harmonics caused by switching are removed. In addition, it can be observed that the machine under investigation exhibits significant harmonic content caused by spatial harmonics.

The measured voltages and currents are first transformed into the dq-system and then filtered using the described method. Subsequently, the differential inductances are determined according to the selected identification method.

C. Identification Procedure

To ensure repeatable and reliable results, the identification process must be standardized, with temperatures either controlled or at least monitored. This is done using a state machine that checks whether the temperatures are within a defined range so that the stator resistance remains approximately constant throughout the identification process. Depending on the thermal mass of the rotor, an additional conditioning phase must be taken into account. The state machine also ensures data acquisition by triggering the power analyzer.

TABLE I: Measurement and Control Equipment

Device Type	Model
Control System	dSPACE Scalexio with the I/O-Cards DS6121 & DS6202
Power Analyzer	HBK Genesis Gen3iA
Current Transducer	LEM IT 400-S Ultrastab
Voltage Transducer	Differential Probe TESTEC TT-SI 8110

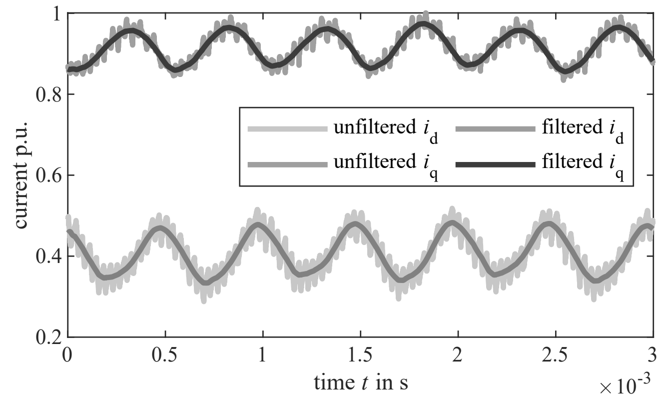

Fig. 3: An example of a measured dq-current combination over an entire electrical period is shown.

D. Finite Element Simulation

FE simulation of PMSMs enables detailed analysis of electromagnetic fields and machine behavior under various operating conditions. The machine model is discretized to numerically solve the field equations. The choice of element size significantly affects both accuracy and computation time. A finer mesh yields more precise results but increases computational effort, whereas a coarser mesh reduces accuracy. In this work, a locked-rotor simulation without iron losses was conducted. For the first machine, simulations were performed over multiple current steps in both the direct and quadrature axes, using a step size of $10\,\%$ of the rated current. Each operating point was evaluated over the full range of electrical angles with a resolution of $1°$. For the second machine, the current step size was set to $8\,\%$ of its rated current.

The differential inductances were transformed into the dq-system as outlined in [5] and were previously obtained via FE simulation using the method described in [15].

V. Results

This section presents and discusses the results, comparing the methods are compared in terms of implementation and analysis effort. The offline identification methods were tested on two different electrical machines: a $400\,\mathrm{V}$ traction drive M1 with a rated power of $40\,\mathrm{kW}$, and a second machine M2, a low-voltage drive with approximately $1\,\mathrm{kW}$.

To compare the identification results of both methods, the differential inductance maps L_{dd}, L_{dq}, L_{qd} and L_{qq} without angle dependency are examined.

The differential inductance maps of M1 are compared with those obtained from both measurement-based methods and FE simulations. In constrast, the high-frequency method failed to produce reliable results for M2. A hypothesis explaining this outcome is discussed in section V-B. Nevertheless, the FE simulation results were succesfully compared with those obtained using the derivative method.

In Figs. 4, 5, and 6, an operating point is highlighted by a red dot. This operating point was selected to facilitate a direct comparison of the inductance estimation results obtained using different methods. A detailed numerical comparison corresponding to this operating point is provided in Table II. It is also important to note that the machines under investigation primarily operate in motor mode. Therefore, only the motor operating quadrant is presented in the corresponding plots. This focus allows for a more relevant analysis of inductance behavior under typical operating conditions, where accuracy in the motor region is of primary interest. While the remaining quadrants are not displayed, they demonstrate similar accuracy.

A. *Discussion of the Derivative Method*

By comparing the differential inductance maps of M1 obtained from measurements with those simulated using the institute's own (FE) solver, *pyMOOSE*, a high degree of agreement between the simulation results and the identified inductances is observed, as illustrated in Fig. 4. Specifically, the inductance L_{qq} exhibits a maximum relative error of $15\,\%$, whereas the deviations for L_{dq} and L_{qd} reach up to $40\,\%$. The closest correspondence is found for L_{dd}, with relative errors within the single-digit percentage range.

The relative error of the inductance maps of M2 between the derivative method and the FE simulation is shown in Fig. 5. The relative error of L_{dq} is approximately $50\,\%$, while the relative error of L_{qd} reaches up to $400\,\%$ at certain points. This deviation may result from high speeds during the identification process, leading to the occurrence of iron losses. Inaccuracies in material modeling may also represent a potential source of deviation in the results. The relative error of L_{dd} remains below $25\,\%$, and for L_{qq}, it varies between $0\,\%$ and $30\,\%$ around zero q-current.

B. *Discussion of the High Frequency Method*

By comparing the differential inductances of M1, determined by the high frequency method and FE simulation, as shown in Fig. 6, it can be seen, that the relative error of L_{dd} is remains in a range from $20\,\%$ to $50\,\%$ over the entire map. The relative error of L_{qq} varies from $30\,\%$ in the outer region at high q-currents and low d-currents, with the error increasing as the d-current decreases.

Since the identification of the differential inductances of M2 was unsuccessful, a possible hypothesis is proposed. In contrast to the present setup, the studies in [12] and [6] utilized machines with significantly higher supply voltages. A closer examination of (16), (17), (18), and (19) reveals that the ratio between $U_{\mathrm{x,HF}}$, $x \in \{d, q\}$, and $I_{\mathrm{x,HF}}$, $x \in \{d, q\}$, plays a crucial role. M2 is a low-voltage machine with low inductance values in the range of several µH, whereas the machine used in [6] features inductances in the mH range. As a result, the voltage-to-current ratio is on the same order of magnitude as the phase resistance, making the identification process highly sensitive to measurement noise, disturbances, and filtering errors. Furthermore, even minor resistance changes due to temperature rise can significantly affect the results. Another contributing factor is the inherent cross-coupling in permanent magnet synchronous machines: injecting a high-frequency signal into one axis inevitably influences the other. This effect

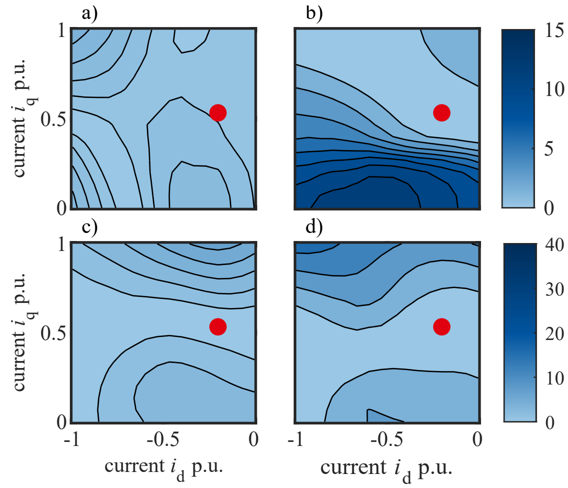

Fig. 4: Comparison of the differential inductances of M1 determined using FE simulations and derived by the derivative method. In a) and b), the relative errors (%) of the self-inductances L_{dd} and L_{qq} are shown, whereas c) and d) present the cross-coupling inductances L_{dq} and L_{qd}. The red dot indicates an exemplary operating point used for comparison.

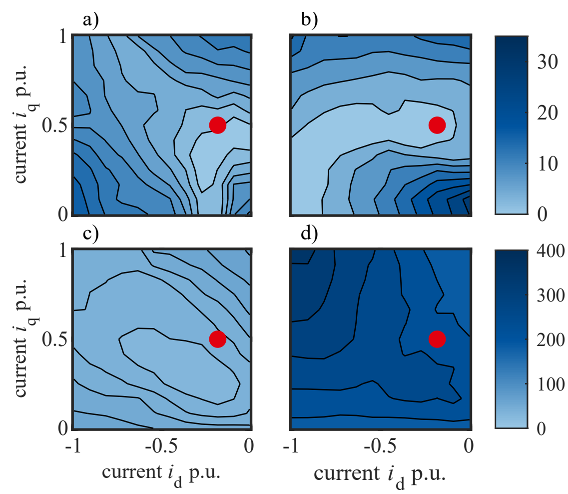

Fig. 5: Comparison of the differential inductances of M2 determined using FE simulation and derived by the derivative method. In a) and b), the relative errors (%) of the self-inductances L_{dd} and L_{qq} are shown, whereas c) and d) present the cross-coupling inductances L_{dq} and L_{qd}. The red dot indicates an exemplary operating point used for comparison.

can only be partially compensated by adjusting the controller parameters.

VI. Summary and Outlook

In this work, two measurement methods were compared, and the results were presented in detail. For machine M1, both measurement-based methods were evaluated against FE simulation results to verify both the accuracy of the FE model and the feasibility of the measurement approaches. For

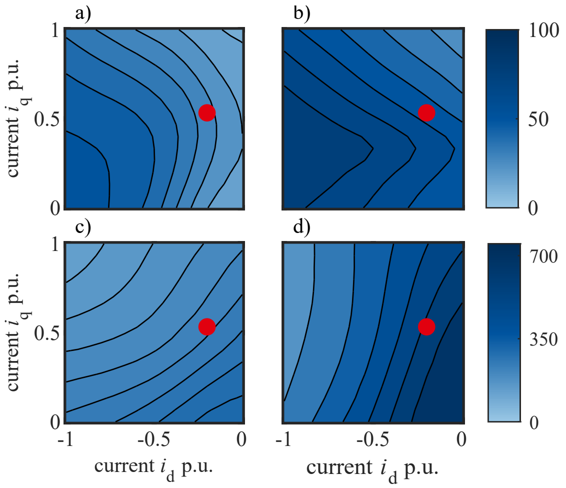

Fig. 6: Comparison of the differential inductances of M1 determined using the institute's own FE solver *pyMOOSE* and derived by the high frequency method. In a) and b), the relative errors (%) of the self-inductances L_{dd} and L_{qq} are shown, whereas c) and d) present the cross-coupling inductances L_{dq} and L_{qd}. The red dot indicates an exemplary operating point used for comparison.

TABLE II: Comparison of Relative Errors (%) for M1 and M2

Machine	Diff. Inductance	Simulation vs. Derivative Method	Simulation vs. High Frequency Method
M1	L_{dd}	0.53	29.14
	L_{qq}	0.01	54.38
	L_{dq}	0.13	236.79
	L_{qd}	0.06	599.09
M2	L_{dd}	2.49	-
	L_{qq}	2.92	-
	L_{dq}	41.47	-
	L_{qd}	224.38	-

machine M2, the derivation method and FE simulation results were compared.

The high-frequency method requires further investigation regarding its applicability to specific machine types and the required boundary conditions. It shows better suitability for machines with larger inductances, which result in a more favorable voltage-to-current ratio compared to the setup used in this study.

From the perspective of measurement effort, accuracy, and applicability, the derivation method proves to be the most straightforward—especially when a speed-controlled test bench is available. Such a setup enables simultaneous identification of flux linkages as functions of currents and rotor position. It also allows investigation of the influence of speed-dependent iron losses on both flux linkages and differential inductances.

The strong correlation between measurement and simulation results enables the early evaluation of various control strategies during the design phase. Overall, the derivation method has shown to be robust, broadly applicable, and easily implementable for a wide range of permanent magnet synchronous machines. In contrast, further research is needed to determine how the high-frequency method can be refined and generalized across different machine types.

References

[1] S. L. Kellner, *Parameteridentifikation bei permanenterregten Synchronmaschinen*. Dissertation, Technische Fakultät, Friedrich-Alexander-Universität Erlangen-Nürnberg, Erlangen, Dec. 2012.

[2] D. C. R. Pinto, A. Douiri, and R. W. de Doncker, "Implementation and Validation of a LUT-Based Model of an IPMSM Considering Saturation and Spatial Harmonics," in *2024 27th International Conference on Electrical Machines and Systems (ICEMS)*, pp. 1196–1204, Nov. 2024. ISSN: 2642-5513.

[3] M. Hepp, M. Saur, W. Wondrak, and M.-M. Bakran, "Enhanced Analytical Models Based on Switching Angles to Evaluate the Effects of Optimized Pulse Patterns on the Overall Electric Drive Train," *IEEE Transactions on Energy Conversion*, vol. 40, pp. 785–796, June 2025.

[4] K. Rehorik, *Enhancing the Fault Tolerance of the Electric Drive in a Future Steering System by Utilizing Self-Sensing*, vol. 53 of *Forschungsberichte Elektrische Antriebstechnik und Aktorik*. Düren: Shaker Verlag, 2023.

[5] T. Herold, D. Franck, E. Lange, and K. Hameyer, "Extension of a d-q model of a permanent magnet excited synchronous machine by including saturation, cross-coupling and slotting effects," in *2011 IEEE International Electric Machines & Drives Conference (IEMDC)*, pp. 1363–1367, May 2011.

[6] R. Kowalski and J. Windelberg, "Anisotropy Identification for Electromechanical Flight Actuators With Sensorless Rotor Angle Detection," *IEEE Transactions on Transportation Electrification*, vol. 6, pp. 1448–1456, Dec. 2020.

[7] A. Brosch, O. Wallscheid, and J. Böcker, "Long-Term Memory Recursive Least Squares Online Identification of Highly Utilized Permanent Magnet Synchronous Motors for Finite-Control-Set Model Predictive Control," *IEEE Transactions on Power Electronics*, vol. 38, pp. 1451–1467, Feb. 2023.

[8] E. Armando, R. I. Bojoi, P. Guglielmi, G. Pellegrino, and M. Pastorelli, "Experimental Identification of the Magnetic Model of Synchronous Machines," *IEEE Transactions on Industry Applications*, vol. 49, pp. 2116–2125, Sept. 2013.

[9] A. Brosch, S. Hanke, O. Wallscheid, and J. Böcker, "Data-driven recursive least squares estimation for model predictive current control of permanent magnet synchronous motors," *IEEE Transactions on Power Electronics*, vol. 36, no. 2, pp. 2179–2190, 2021.

[10] K. Rahman and S. Hiti, "Identification of machine parameters of a synchronous motor," *IEEE Transactions on Industry Applications*, vol. 41, pp. 557–565, Mar. 2005.

[11] S. Decker, J. Richter, and M. Braun, "Predictive current control and online parameter identification of interior permanent magnet synchronous machines," in *2016 18th European Conference on Power Electronics and Applications (EPE'16 ECCE Europe)*, pp. 1–10, Sept. 2016.

[12] S. Ebersberger and B. Piepenbreier, "Identification of differential inductances of permanent magnet synchronous machines using test current signal injection," in *Automation and Motion International Symposium on Power Electronics Power Electronics, Electrical Drives*, pp. 1342–1347, June 2012.

[13] S. L. Kellner and B. Piepenbreier, "General PMSM d,q-model using optimized interpolated absolute and differential inductance surfaces," in *2011 IEEE International Electric Machines & Drives Conference (IEMDC)*, pp. 212–217, May 2011.

[14] M. X. Bui, R. Dutta, and F. Rahman, "Application of Deep Learning in Parameter Estimation of Permanent Magnet Synchronous Machines," *IEEE Access*, vol. 12, pp. 40710–40721, 2024.

[15] E. Lange, F. Henrotte, and K. Hameyer, "An efficient field-circuit coupling based on a temporary linearization of fe electrical machine models," *IEEE Transactions on Magnetics*, vol. 45, no. 3, pp. 1258–1261, 2009.